# Semi-Keplerian Magnetized Accretion-Ejection Structures

Seyedeh Zeynab Mousavi[*1] · Alireza Khesali[2] · Azar Khosravi[3]

1   Department of physics, University of Mazandaran, Babolsar, Iran;
    *email: sz_mousavi35@yahoo.com
2   Department of physics, University of Mazandaran, Babolsar, Iran;
    email: khesali@umz.ac.ir
3   Department of physics, University of Mazandaran, Babolsar, Iran;
    email: a.khosravi@umz.ac.ir

**Abstract**. It was previously found that the structure of a thin geometrically axisymmetric stationary disk around a central black hole threaded by a bipolar magnetic field drives jets by extracting angular momentum. In this work, it is assumed that the effect of viscosity turbulence is negligible. If the effect of viscosity turbulence is negligible and the lines of the initial magnetic field have the required curvature, the magnetic force can be the only factor that determines the material leaving the disk. A primary poloidal magnetic field is applied to the disk, which has two components of $r$ and $z$. The equations that describe the vertical structure of the disk in a cylindrical system have been solved. We assume that the angular velocity is not completely Keplerian and the deviation from the Keplerian rotation enters the equations. It was seen that for a smaller ejection rate (a smaller $\zeta$), the deviation from the Keplerian rotation is greater. The vertical structure equations of the disk were written with the presence of the polytropic equation. The gas with polytropic state equation with different gammas is given in this paper. For all gases, the variation in the toroidal magnetic field in the vertical direction is similar and for a constant ejection rate, the monoatomic gas has a greater deviation from the Keplerian rotation. Our results show that in the presence of the polytropic equation and the deviation from Keplerian rotation, the process of mass reduction in the vertical direction for diatomic gas occurs faster.

*Keywords*: Accretion disks, Magnetic fields, Keplerian rotation, Magnetized accretion-ejection Structure.

## 1   Introduction

Accretion disks are an old astronomical phenomenon [22] and can be seen in a wide range of physical astronomical models such as the formation of stars, binary stars, galaxies, and galactic nuclei [23]. Astrophysical jets in the form of high-velocity streams of matter have been seen as a common phenomenon in many astronomical sources, such as young stars, quasars, and active galactic nuclei [7]. What has been learned so far is that these fast jets originate from a system consisting of a massive central black hole surrounded by an accretion disk. The magnetic fields that surround the accretion disk play an important role in the formation and propagation of the jet. Several models explain the formation of such jets. Ferreira & Pelletier [9], has told that in these models, the opened magnetic field lines thread the accretion disk and the field lines are twisted by the differential rotation of the plasma; thus, a toroidal component of the magnetic field is created: 1. This component exerts braking torque that transmits angular momentum. 2. This component creates an

MHD pointing flux related to the centrifugal acceleration of the rotating material, which flows along the flux tubes. 3. Magnetic tension is responsible for self-collimation of the flow. The first self-similar analytical solution of this kind was extracted by [2] under certain assumptions.

It was suggested by [24] that such a wind could remove all the angular momentum of the accreting material and control the accrete current without the need for turbulence viscosity. The jet properties that extract all the angular momentum of the disk through the MHD mechanism were extensively studied by [19–21]. [20] describes the structure of a jet-producing magnetized accretion disk that emits all its angular momentum without any effect of viscosity which is connected to the internal part of an accretion disk that has Thomson opacity and is supported by radiative pressure.

[11] have shown that the only required stable configuration is an accretion disk in which there is an equilibrium between thermal and magnetic pressure to prevent very strong magnetic compression and magnetic rotational instability. Some self-similar studies, model both the accretion disk and the super Alfvenic jet in a stationary framework using the method of separating variables with different levels of assumptions [3,4,9–11,13,16,17,26]. [5] present 2.5-dimensional MHD time-dependent Calculations starting from an initial configuration close to a self-similar configuration. They presented MHD calculations that showed the launching of superfast and magnetosonic, collimated jets from a resistive accretion disk over a large number of dynamic time scales [6]. One of the best attempts to create an accretion-ejection structure in time-dependent simulations has been made by [5,6] which showed how a quasi-stationary jet can be launched from the equipartition areas of a resistive accretion disk.

For a magnetized accretion disk structure, the first time-dependent numerical simulations by [25] or [15] showed that the interaction between a geometrically thin rotating disk and a large-scale magnetic field is at first uniform and vertical and generates a position that creates a strong toroidal field and projects the material perpendicular to the disk surface. Some important researches related to jet-disk simulation have been done in [5,25,27–34]. In [27] an analytic self-similar equilibrium configuration of the disk including gravitational forces, centrifugal force, thermal pressure, and Lorentz force is solved. There are papers of jet formation defined in axisymmetric setup using simulations (e.g., [8,35,36]) in which the axisymmetric MHD simulations of jet emission in a finite gas have been performed using the PLUTO code.

The 3D numerical simulations (for jet 3D simulation see e.g. [37–43]; and for 3D disk-jet simulation [32–34] show that if there is no large-scale vertical magnetic field, there is magnetic rotational instability and the accretion continues but no jet is launched [1], see however [18]. So launching jets processes from accretion disks that carry mass, energy; and, angular momentum requires the presence of a large-scale vertical field. It should be noted that in this case, whatever the relative importance of the jet torque to the turbulence torque, a steady accretion occurs only if the disk material is allowed to propagate through the magnetic field [14]. They believe that the important physical parts that should be in an accretion-ejection model include the following

1. A disk of plasma that rotates almost near-keplerian and surrounds the central body.

2. Large-scale magnetic field that threads the disk.

3. Mass propagation through the field must be considered, meaning that part of the accreting mass falls into the central object and the rest is delivered to the jet through the magnetic field.

In previous papers written by other authors on this subject, the problem of accretion-ejection self-consistently was formulated [9] and partially solved for the situation where the magnetic Reynolds number is of order one and the magnetic surfaces are direct [10]. In such cases, the corona heating of the disk is used to allow the material to escape, since the slope of the field line more than 30 degrees from the vertical axis is required for the escape of cold matter [2]. [11] presents general solutions with higher magnetic Reynolds numbers so that the magnetic surfaces are sufficiently curved and allow about 1% to 80% of the total disk matter to ejection.

Here, we continue with high Reynolds numbers so the magnetic surfaces are curved enough but the polytropic equation is used with different gammas, while the deviation from Keplerian rotation is considered. Here, we examine the effect of deviation of keplerian rotation with the polytropic equation and study the results of these two effects on the equations simultaneously.

The paper is organized as follows. In section 2, we describe a complete set of equations governing a magnetized accretion disk threaded by open magnetic field lines. In section 3, we write the modeling of the disk structure and parameter constraints. In section 4, we write the equations after dimensionless process and perform the mathematical operations. The differential equations describe the vertical structure of the disk both in the region of the resistive inner disk and in the ideal MHD outer layers. Section 5 describes how to work on the equations by using the Self-similarity method. In section 6, conclusions are given.

## 2  MHD equations and basic assumptions

We consider a thin geometrically axisymmetric ($\frac{\partial}{\partial \varphi} = 0$) stationary disk around a central black hole threaded by a bipolar magnetic field. The magnetic field is described by two scalar functions: $b(r,z) \equiv B_\phi(r,z)$ such that $b(r,-z) = -b(r,z)$ and $a(r,z)$ such that $a(r,-z) = a(r,z)$ which is a magnetic flux through the circular surface of radius $r$ centered on the axis at the height $z$. The poloidal component of the magnetic field can derive from $a(r,z)$

$$\mathbf{B}_P = \frac{1}{r}\nabla a \times \mathbf{e}_\phi, \tag{1}$$

and toroidal component is introduced by

$$b(r,z) = rB_\phi. \tag{2}$$

The continuity equation is

$$\frac{1}{r}\frac{\partial}{\partial r}(\rho r u_r) + \frac{\partial}{\partial z}(\rho u_z) = 0, \tag{3}$$

which, can be integrated vertically over the surface of the disk

$$\zeta = \frac{d\ln}{d\ln r}\left(\frac{\dot{M}_a(r)}{\dot{M}_{ae}}\right). \tag{4}$$

The relationship between the inward mass flux, $\dot{M}_a(r)$, and the ejection rate, $\dot{M}_j(r)$, which is outward mass flux and is integrated from the inner radius $r_i$ to the radius $r$. The total ejection rate depends only on the radial extension of the disk and a parameter called the ejection index in equation (3). This index can be expressed according to radial exponents (see equation(42) of [9]). This ejection index is an important control parameter for the outflow. We take this ejection index as /1 and /15.

The radial equilibrium, which is mainly due to the balance of the gravitational attraction with the centrifugal force, is characterized by the Keplerian velocity proportional to $r^{-\frac{1}{2}}$, see e.g. [47]. The vertical equilibrium can be a balance between gravitation and toroidal magnetic pressure. It is assumed that the magnetic field is not strong enough to perturb Keplerian balance and the angular velocity with relation $r^{-\frac{3}{2}}$ depends on the radius.

[11] say in comparison with the Lorentz force and the pressure gradient, the radial acceleration is ignored because these two forces are in front of gravity, they reduce the speed of rotation and the speed becomes slightly subkeplerian. It should be noted that because the magnetic effect increases with decreasing density, the angular velocity decreases with altitude, causing $\nabla\Omega \prec 0$ inside the disk but do not assume that the material rotates on the surface of the disk much slower than the center plate of the disk. As the acceleration along the magnetic field lines increases, the centrifugal section overcomes the other sections and the rotation becomes super-keplerian. They say this effect reflects the magnetic field's increasing ability to conduct current, which reaches a high magnetic Reynolds number at the top of the disk. Matter attaches to field lines that are anchored to the inner radii and therefore rotate at greater speeds. Therefore, this deviation is sometimes sub-Keplerian and sometimes super-Keplerian, and the vertical variation of this deviation has been investigated.

Note that the vertical variation of angular velocity can be ignored only if the field lines are almost straight inside the disk. One of the important cases that has been studied in this paper is the study of deviation from Keplerian rotation. We want to see how the parameters of the disk change in the presence of deviation from Keplerian rotation. But the deviation from Keplerian rotation can be examined for two reasons: its importance in the angular momentum transport and the production of the toroidal field.

$$\Omega = \Omega_k \left(1 + \omega\right), \tag{5}$$

with $\omega \ll 1$. The transport equation of the radial momentum for this angular velocity shift is [11]

$$\left(\mathbf{u}_p.\nabla\right) u_r - 2\omega\Omega_k^2 r + \frac{1}{\rho}\frac{\partial p}{\partial r} = \frac{1}{\rho}\left(J_\phi B_z - J_z B_\phi\right). \tag{6}$$

If the magnetic field lines are almost directly inside the disk, the vertical variation of the angular velocity can be ignored, which we should considere here because the magnetic field lines are not straight, ie we are dealing with high magnetic Reynolds numbers.

The angular momentum transport equation is as follows

$$\nabla.\left(\rho\Omega r^2\mathbf{u}_p - \frac{b}{\mu_0}\mathbf{B}_p\right) = \frac{1}{r}\frac{\partial}{\partial r}\left(r^2\tau_{r\phi}\right). \tag{7}$$

When the magnetic torque dominates the viscous torque, this equation becomes

$$\frac{1}{2}u_r\left(1 + \omega\right) + u_z r\frac{\partial\omega}{\partial z} - \frac{J_z B_r - J_r B_z}{\rho\Omega_k} = 0. \tag{8}$$

A quasi-hydrostatic equilibrium is obtained when the plasma pressure gradient balances the confining force which in standard accretion disk theory is the gravity force due to the central object while self-gravity is ignored. However, in magnetized accretionejection structures, the magnetic pressure of the toroidal and radial components works, as well as the magnetic tension due to $B_z$ to confine the material of the disk. This makes such disks thinner than disks that are purely hydrodynamic and leads to an internal area in magneto-hydrostatic equilibrium

$$\frac{\partial p}{\partial z} \simeq \rho\Omega_k^2 z + J_r B_\phi - J_\phi B_r. \tag{9}$$

Therefore, any vertical motion results from a deviation from this balance in the inner part of the disk. In this quasi-static part of the disk near the mid-plane, the vertical motions are only due to the plasma pressure gradient and not to any MHD acceleration effect.

There is an equation that describes the equilibrium between the diffusion processes and the advection of the magnetic field with the flow. This equation is derived from Maxwell's equations and Ohm's law.

Without considering the effects of diffusion within the disk, a stationary state is not achieved for the disk. Therefore, effective transport coefficients such as magnetic diffusivity $\nu_m$ and resistivity $\eta_m = \mu_0 \nu_m$ due to turbulence sources within the disk must be considered. There are diffusion processes that allow the matter to slip through the lines of the magnetic field.

$$\eta_m J_\phi = \mathbf{u}_p \times \mathbf{B}_p, \tag{10}$$

$$J_\phi = -\frac{1}{\mu_0 r} \Delta' a, \tag{11}$$

$$\Delta' = r \frac{\partial}{\partial r} \frac{1}{r} \frac{\partial}{\partial r} + \frac{\partial^2}{\partial z^2}. \tag{12}$$

The balance between the advection of the toroidal component and the differential rotation (both vertical and radial) is corrected by the diffusion inside the disk

$$\Delta . \left( \frac{\nu'_m}{r^2} \Delta b \right) = \Delta . \frac{1}{r} \left( B_\phi \mathbf{u}_p - \mathbf{B}_p \Omega r \right). \tag{13}$$

From these equations, a magnetic Reynolds number can be defined that characterises the radial transport of the magnetic field by the accretion flow, namely $\Re_m \equiv r_e u_{re}/\nu_{me}$ where the subscript $e$ refers to the values at $r_e$, the radius of the outer opened magnetic flux tube, measured on the equatorial plane. It can be noted that this Reynolds number is of order unity for a smoothly bent magnetic field, whereas for a strongly bent field it is much larger.

The difficulties on modeling steady state magnetized accretion disks increase when progress towards more realistic description are attempted. The simplest modeling consists in solving the induction equation for the jet alone, decoupled from the other transport equations in the disk but allowing to derive some constraints on the magnetic field topology [44–47]. The jet equations are written in the ideal MHD regime, and therefore the diffusivity effects are negligible. According to $\Re_m \equiv r_e u_{re}/\nu_{me}$, the magnetic Reynolds number will be high in this case. There is a close relationship between the magnetic Reynolds number and other disk parameters, which we will mention in the rest of the paper.

In this work, it is assumed that the effect of viscosity turbulence is negligible. If the effect of viscosity turbulence is negligible and the lines of the initial magnetic field have the required curvature, the magnetic force can be the only factor that determines the material leaving the disk. $\nu'_m$ is the magnetic toroidal diffusivity that is slightly different from the magnetic poloidal diffusivity $\nu_m$ [11] and we have taken it to be zero in equations.

To close the system, we need an energy equation which we replace with a simple polytropic equation.

$$p = k\rho^\gamma, \tag{14}$$

$\gamma = \frac{C_P}{C_\nu}$ is the ratio of specific heats and $K$ is a constant related to the speed of sound by $c_s^2 = k\gamma\rho^{\gamma-1}$. In this work, we consider different values for gamma.

Ferreira and Pelletier [9], showed that the TC disk model (dominant toroidal current) scales the central temperature to $r^{-\frac{3}{8}(1-4\zeta)}$, $\zeta$ is ejection rate, which for small $\zeta$ is almost the

same as the standard Shakura and Sanyo models (or the radiative $\alpha PTC$-disk, see Ferreira & Pelletier 1993a, where $\alpha_6 = -\frac{3}{8}$ and $\alpha_6$ is the exponent of the radial part of the temperature profile).

But the standard disk in this case (radiative), shows that the thickness changes of the disk with radius are constant. [10] claimed that ignoring vertical motions would cause the photosphere to behave differently from what it had previously found to be and they said that a sharp change in the actual surface of the disk creates an effective temperature in the photosphere that is different from the central temperature.

The vertical structure of temperature depends on the dominant heat transport mechanism. An adiabatic description can be used for a convective disk, or a vertical temperature profile can be considered for a radiative disk (the inner radiative region of AGN where opacity is dominated by electron scattering), in which case the temperature gradient should not be too sharp because convection occurs. Therefore, the assumption that the temperature is constant in the vertical direction is incorrect [11]. They showed that jets could only be produced by magnetic effects.

For such jets, the vertical temperature profile does not have much effect on the plasma dynamics, so the isothermal version can be used because most of the accretion power enters the jet in the form of MHD pointing flux. Thus, magnetically driven jets are seen with weakly dissipative disks, where thermal effects can be ignored [12].

# 3    Modelization of the disk structure

In dimensionless process of the original equations, we normalized all the values to the values at the disk mid-plane. [9] states that different physical values have a radial dependence on $r$ in the equatorial plane. Except for the gravitational field and the poloidal magnetic field (if the Reynolds number is of order unity) which have a smooth vertical variation inside the disk, all other values vary on the scale $h(r)$. So, it is natural to look for self-similarity solutions as a product of the power of $r$ multiplied by a function of $x \equiv z/h(r)$. We use all the functions introduced in [9] except $T(r,z)$ because temperature is not explicitly used in the polytropic equation. So the following functions are defined, after reducing all the quantities with respect to their value at the external radius $r_e$.

1. $p(r,z) = p_e(r/r_e)^{\alpha_0} f_0(x)$, where $f_0$ is an even function such that $f_0(0) = 1$.

2. $b(r,z) = r_e B_{\phi e}(r/r_e)^{\alpha_1} f_1(x)$, where $f_1$ is an odd function.

3. $u_r(r,z) = -U_e(r/r_e)^{\alpha_2} f_2(x)$, where $f_2$ is an even function such that $f_2(0) = 1$.

4. $u_z(r,z) = V_e(r/r_e)^{\alpha_3} f_3(x)$, where $f_3$ is an odd function.

5. $\rho(r,z) = \rho_e(r/r_e)^{\alpha_4} f_4(x)$, where $f_4$ is an even function such that $f_4(0) = 1$.

6. $\nu_m = \nu_e(r/r_e)^{\alpha_5} f_5(x)$, where $m$ is an even function such that $m(0) = 1$.

7. $h(r) = h_e(r/r_e)^{\alpha_7}$.

The disk radial structure is described by a set of radial exponents $\alpha_i$ that are almost constant with the radius, if a magnetized accretion-ejection structure is established through a wide range of radii. These exponents (and among them, are the flux distribution $\beta$ and the ejection index $\eta$) depend directly on the density exponent, which in turn, is provided by the energy balance equation (see section 5 [9]).

So, we solve the following set of ODE equations that describe the vertical structure of the disk from the disk mid-plane to a given altitude above the disk. The flux function is written as follows

$$a(r, z) = a_e \left( \frac{r}{r_e} \right)^\beta \psi(x), \tag{15}$$

where $a_e = B_z(r_e, 0) r_e^2 / \beta$ is related to the total magnetic flux that $\phi$ threads the disk into its mid-plane

$$\phi = 2\pi a_e \left( 1 - (r_i/r_e)^\beta \right). \tag{16}$$

## 3.1   Parameter constraints

The dimensionless parameters describing magnetized accretion disks are

1. The thin disk approximation is insured with $\varepsilon = h/r$ smaller than unity, while the disk scale height is defined by the characteristic pressure scale of variation by setting

$$h^2 = \frac{P_0}{\rho_0 \Omega_k^2}, \tag{17}$$

where the subscript "0" refers to values defined at the disk equatorial plane.

2. The strength of a magnetic field must be comparable to the strength of the tidal force, not the force of gravitational, so the ejection requires magnetic effects that overcome the tidal compression. This relationship is shown by the parameter

$$\mu = \frac{V_{A_0}^2}{\Omega_k^2 h^2}, \tag{18}$$

which shows the relative strength of these two effects on the vertical direction.

3. The level of turbulence that is required to obtain the magnetic diffusivity allowing an extraction of angular momentum is parametrized by $\alpha_m(\alpha_m \geq 1)$. The parameter $\alpha_m$ is easy to constrain and stands here for the shear parameter

$$q = \frac{\alpha_m}{2} (1 + \omega_0) \frac{rh}{\beta l^2} \mu^{-1/2}, \tag{19}$$

($\omega_0$ is the departure from the Keplerian rotation at the disk mid-plane, $l$ is magnetic field scale height). This shear parameter controls the radial current responsible for the magnetic braking, as in a Barlow wheel.

4. The poloidal velocity is measured with respect to the sonic velocity, so that the sonic Mach number measured at the disk equatorial plane, writes

$$m_s = \frac{\mu_0}{C_{s0}} = \frac{2q\mu}{1 + \omega_0} = \alpha_m \mu^{1/2} \frac{rh}{\beta l^2}, \tag{20}$$

where $\omega_0 = -1 + \sqrt{1 - (\Re_m \mu - \alpha_2 m_s^2 - \alpha_0)\varepsilon^2}$ is the shift from the Keplerian angular velocity measured at the disk equatorial plane.

# 4 The set of non-ODEs describing the disk vertical structure

The following part is a complete set of equations governing a magnetized accretion-ejection system that the prime sign refers to the derivative relative to $x$.

1. Continuity equation

$$f_4' (f_3 + xf_2) - \zeta f_2 f_4 + f_4 (f_3 + xf_2)' = 0. \tag{21}$$

   This equation shows the dependence of the vertical acceleration on the ejection index,

$$f_3'(0) = \zeta - 1. \tag{22}$$

2. Radial momentum transport

$$
\begin{aligned}
m_s^2 \varepsilon^2 f_4 [\alpha_2 f_2^2 + f_2'(f_3 + xf_2)] = & -2f_4\omega + \varepsilon^2 (\alpha_0 f_0 - xf_0') \\
& + q^2\mu^2\varepsilon^2 f_1 (\alpha_1 f_1 - xf_1') \\
& + \frac{\mu^2}{\beta^2}\Delta'\psi (\beta\psi - x\psi').
\end{aligned}
\tag{23}
$$

3. Angular momentum transport

$$2f_4(f_3 + xf_2)\omega' = f_2 f_4(1 + \omega) + \left(\psi f_1' - \frac{\alpha_1}{\beta}f_1\psi'\right)(1 + \omega_0). \tag{24}$$

4. Vertical momentum transport

$$m_s^2\varepsilon^2 f_4 \left[-\alpha_3 f_2 f_3 + f_3'(f_3 + xf_2)\right] = -xf_4 - f_0' - q^2\mu^2 f_1 f_1' - \frac{\mu^2}{\beta^2\varepsilon^2}\psi'\Delta'\psi. \tag{25}$$

5. The diffusion of poloidal flux in the resistive inner disk is as follows

$$m_p\Delta'\psi = -\Re_m\varepsilon^2 \left[\beta f_2\psi - \psi'(f_3 + xf_2)\right], \tag{26}$$

   where $m_p$ is the vertical profile of the poloidal magnetic diffusivity, Where the lines of the poloidal field become frozen in the plasma $(m_p = 0)$, this equation becomes

$$\psi' = \beta\psi f_2(f_3 + xf_2)^{-1}, \tag{27}$$

   and the toroidal current profile becomes

$$\Delta'\psi \equiv \psi''(1 + \varepsilon^2 x^2) - \varepsilon^2 \left[\beta(2 - \beta)\psi + (2\beta - 3)x\psi'\right]. \tag{28}$$

6. The radial current profile in the resistive inner disk is as follows

$$
\begin{aligned}
(m_t f_1')' = & -\Gamma_0 \left[\frac{3}{2\beta}\psi'(1 + \omega) + \psi\omega'\right] \\
& + \Re_m^t\varepsilon^2[(2 + \alpha_4 - \alpha_1)f_1 f_2 \\
& + (f_3 + xf_2)(f_1' - f_1 f_4'/f_4)],
\end{aligned}
\tag{29}
$$

   where $\Gamma_0 = \Re_m^t/qm_s$ and $\Re_m^t$ is the magnetic Reynolds number defined with the toroidal diffusivity. The vertical profile is $m_t$. If we consider the diffusion to be negligible $(m_t = 0)$, the toroidal field advection balances the differential rotation [11]

$$(f_3 + xf_2)f_1' = (f_3 + xf_2)f_1 \left(\frac{f_4'}{f_4} - \frac{3 + \alpha_4}{2\beta}\frac{\psi'}{\psi}\right) + \frac{1}{qm_s\varepsilon^2}\left(\frac{3}{2\beta}\psi'(1 + \omega) + \psi\omega'\right). \tag{30}$$

7. The polytropic state equation

$$f'_0 = \gamma f_4^{\gamma-1} f'_4. \tag{31}$$

We use different gammas here.

# 5  Self-similar solutions and results

We solved a set of differential equations describing the vertical structure of the disk (in section 4) by the Finite Difference numerical method. In this method, the derivatives of the functions are approximated by their equivalent differences. The basis of this method for solving equations is to use the function approximation with the Taylor method.

There are three different physical regimes, governed by the magnetic scale height $l(r)$.

i) If the field lines are almost vertical inside the disk, that is $l \sim r$ or equivalently $\Re_m \sim 1$, the Lorentz force can be neglected in the inner part of the disk ($\omega_0 \sim \mu\varepsilon^2$), unless $\mu \sim r/h$. Such a configuration was studied in [10], in the context of a radiative disk around a compact object.

ii) For $l \sim h$, or $\Re_m \sim \varepsilon^{-2}$, the poloidal field is bent on the disk scale height. Such a configuration is usually used in modeling the jets issued from an accretion disk (e.g., [44]), since it is thought that it provides a more efficient acceleration. Although frequently claimed, such a configuration is probably unstable and leads to a non-steady accretion and ejection.

iii) Intermediate bending, $l \sim \sqrt{rh}$ or $\Re_m \sim \varepsilon^{-1}$ seems to be the most promising configuration. Indeed, for a moderate poloidal field, $\varepsilon \leq \mu \leq 1$ , the disk is in a quasi-steady state with respect to buoyancy and resistive instabilities. Moreover, the magnetic field components are roughly of equal strength at the disk surface and both the radial and the toroidal currents are relevant, implying then the treatment of all the terms in the equations. Hereafter, we will focus only on this MHD configuration.

As can be seen from this analysis, the magnetic Reynolds number is directly linked to the scale height parameter $\varepsilon$, while there is a close connection between the strength of the poloidal field $\mu$ and $\Re_m$. It can be easily understood from the requirement of ejection, that the more curved the field lines, the bigger the magnetic pinching force. Henceforth, the vertical component of the magnetic field cannot be too strong or it will prevent any vertical balance by the plasma pressure, a situation that will lead to a global converging motion of the matter towards the mid-plane of disk. A precise adjustment of $\mu$, according to a given $\Re_m$ and $\zeta$ (that measures the vertical acceleration at the disk mid-plane, see Appendix B of [11]) is then required. For a certain value of $\mu$ and $\zeta$, we have examined the changes of density according to $X$, for different values of the adiabatic index which is shown in figure 5.

As we move from the dense disk to the dilute corona, the density decreases which is expected. Gamma represents different states of gas. This diagram also shows that in the smaller gamma, the ideal classical diatomic gas ($\gamma = 2/3$), the density decreases faster. Of course, the difference between the isothermal state ($\gamma = 1$) and the classical monoatomic gas ($\gamma = 5/3$) is smaller. In another graph (figure 5), the density in terms of $x$ is plotted from another perspective for different $\zeta$. [11] state that when the magnetic pinching force increases, the density at the surface of the disk decreases to lower the ejection rate (a smaller $\zeta$). In this figure for different ejection index values, there is not much difference in the density graph, and the density at the disk surface drops. This is true for all gammas.
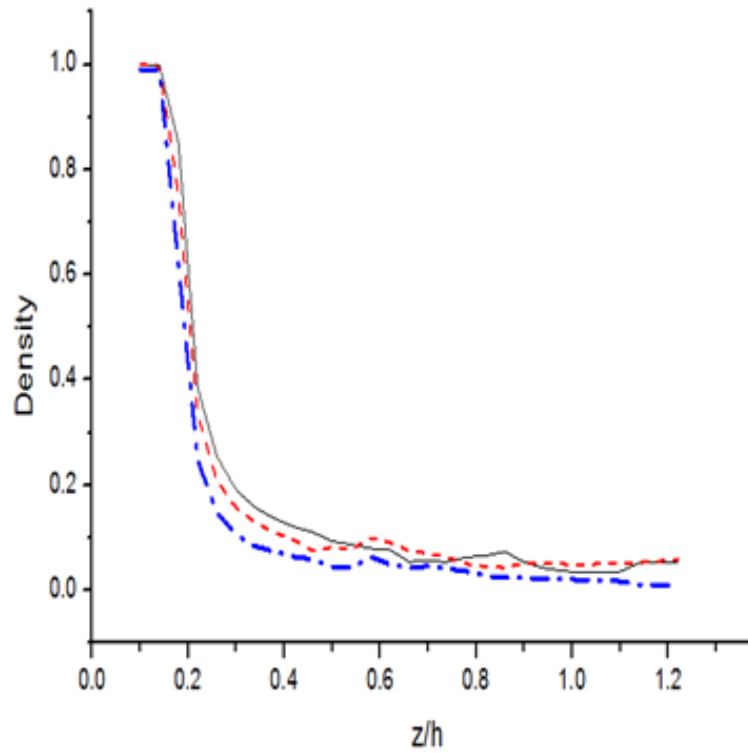
Figure 1: The disk density, normalized by its value in the mid-plane of the disk. This figure is plotted for different gamma values: $\gamma = 1$ (dash line); $\gamma = 2/3$ (dash-dotted line); $\gamma = 5/3$ (solid line).
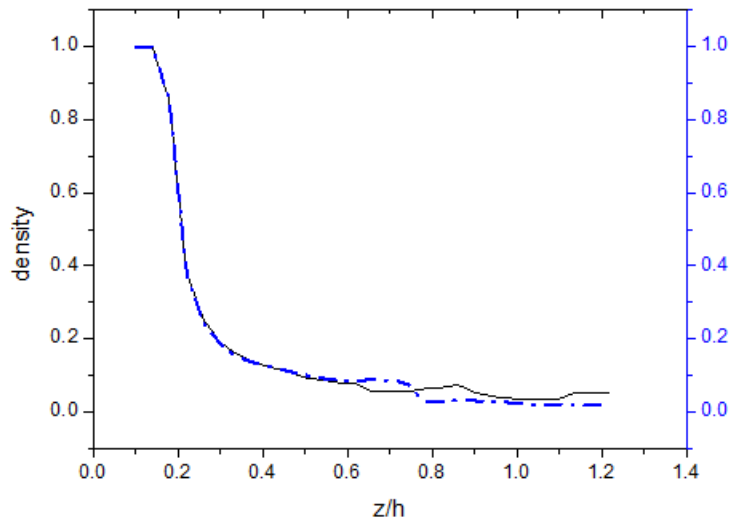


Figure 2: The disk density, for $\varepsilon = 0.1$, and for various values of the ejection index $\zeta$ : $\zeta = 0.1$ with $\mu = 0.698$ (solid line); $\zeta = 0.15$ with $\mu = 0.609$ (dash-dotted line).
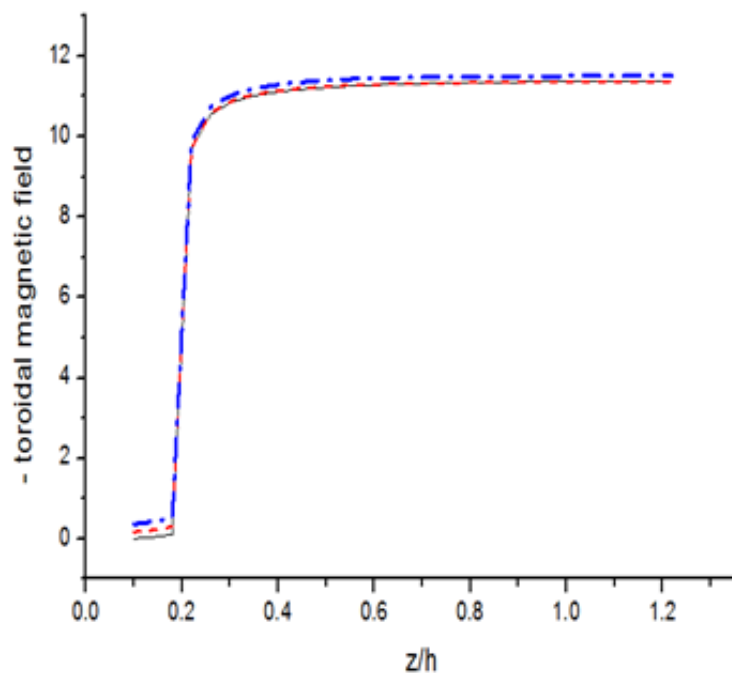
Figure 3: The toroidal magnetic field, for $\gamma = 5/3$ (solid line); $\gamma = 1$ (dash line); $\gamma = 2/3$ (dash-dotted line).

The toroidal component of the magnetic field and its vertical variation (the radial current $J_r$) have tremendous importance on the disk vertical structure, for they are responsible for both accretion and ejection mechanisms. This toroidal component has two different origins: one is the differential rotation of the disk matter and contributes mainly in the ejection process, while the other one is the electromotive force due to the poloidal field that crosses the rotating disk and generates a radial current. This last effect extracts angular momentum from the disk and thus allows the accretion process. The general motion of the plasma is that it falls towards the mid-plane of the disk and at the same time towards the central object. Because of the increasing radial tension of the field (figure 5), the matter is slowed down until the disk surface. Figure 5 shows that for different amounts of gamma, the toroidal magnetic field undergoes a process. This means that in monoatomic gases, diatomic gases, and isothermal gases, after initial widening, the flux tubes explicitly bend towards the jet axis, forcing the matter to flow along them. Of course, in Figure 7 of [11], the toroidal component of the magnetic field, after the initial increase, has a significant bend towards the x-axis ($x = \frac{z}{h}$), but this bend is not observed here.

In most papers on the accretion-ejection structures, it is assumed that the magnetic field is not strong enough to cause a significant deviation from the Keplerian rotation and the material in the disk rotates at an $\Omega = (\frac{GM}{r^3})^{\frac{1}{2}}$ angular velocity ($M$ is the mass of a black hole). If the toroidal and poloidal magnetic energies are negligible compared to gravitational energy, the condition of Keplerian rotation is met [9].

For a constant ejection rate (Figure 5), the monoatomic gas has a greater deviation from the Keplerian rotation, after that, the isothermal gas and finally the diatomic gas. This deviation is reduced at the disk surface.
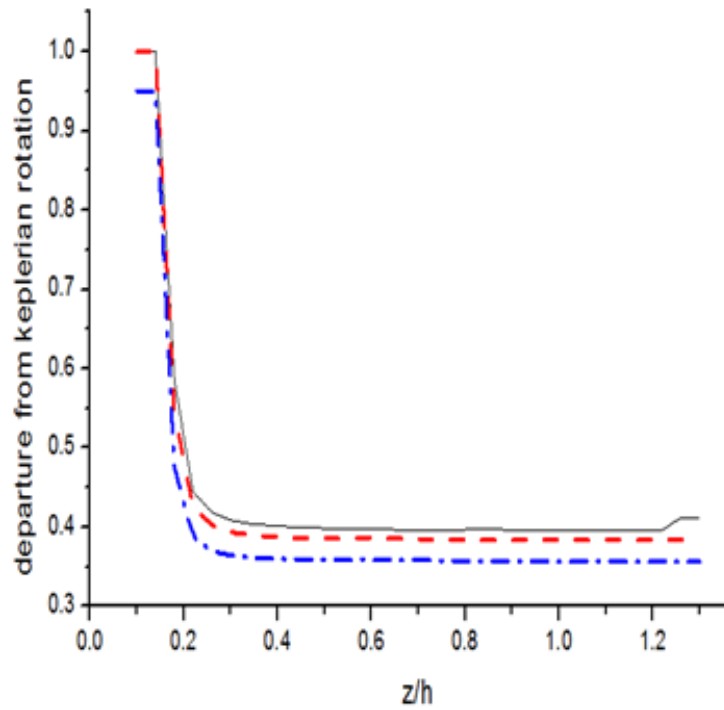
Figure 4: The deviation from keplerian rotation, for and different gamma values. $\zeta = 0.1$ (solid line); $\gamma = 1$ (dash line); $\gamma = 2/3$ (dash-dotted line).
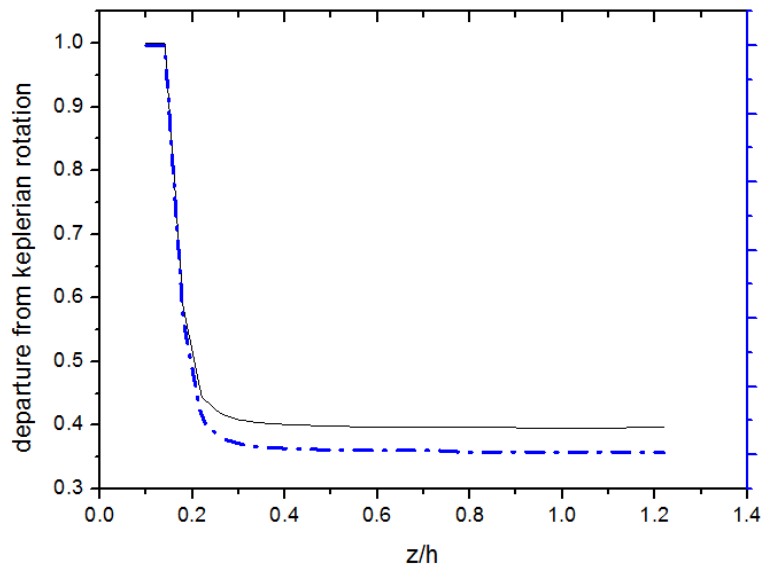


Figure 5: The deviation from keplerian rotation, for $\varepsilon = 0.1$, and for various values of the ejection index $\zeta$ : $\zeta = 0.1$ with $\mu = 0.698$ (solid line); $\zeta = 0.15$ with $\mu = 0.609$ (dash-dotted line).
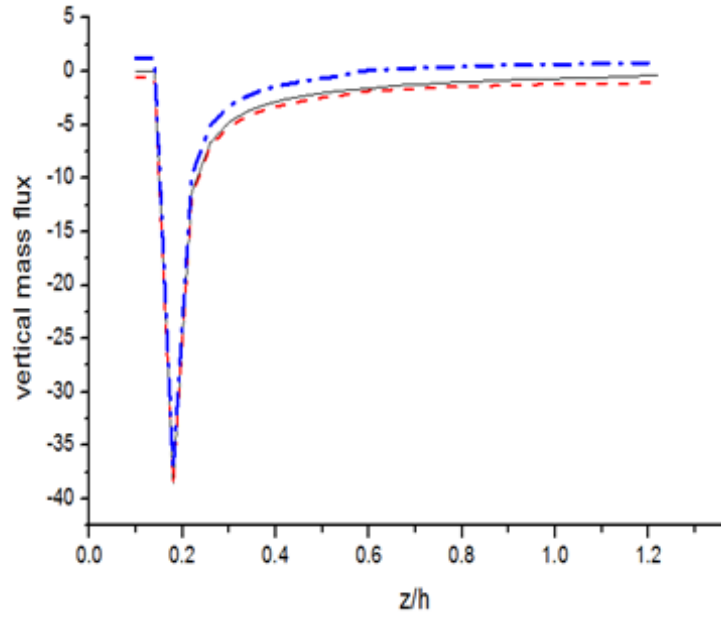
Figure 6: The variation with $x$ of the vertical mass flux $\rho\mu_z$, normalized by $\rho_0\varepsilon U_0$, where $U_0$ is the accretion velocity at the disk mid-plane. For $\zeta = 0.1$ and for various values of the gamma. $\gamma = 5/3$ (solid line); $\gamma = 1$ (dash line); $\gamma = 2/3$ (dash-dotted line).

This diagram shows that for a smaller ejection rate (smaller $\zeta$), the deviation from the Keplerian rotation is greater.

As we move up from the mid-plane, the mass flux moves to the top of the disk, which indicates that the mass exits in a vertical direction. The amount of output mass flux (figure 5), in the vertical direction for different gamma values, does not show a significant difference.

## 6  Conclusion

In general, it is important to study the accretion disks with magnetically driven jets. Jets can participate in the angular momentum transport (by carrying mass outward) and affect the disk structure. [11] considered a magnetized accretion-ejection structure that explained the physical processes and conditions that allow the steady-state launch of the jet and examined the properties of this magnetized accretion-ejection structure.

While in many systems the disk rotation is not keplerian and there is a deviation from the keplerian rotation, this deviation is ignored and no distinction is made for the polytropic index for different gases. This made us interested to investigate the model of Ferreira to re-examine the vertical structure of the disk by adding the polytropic equation and examining the polytropic index in the equations. We think that if all these effects are applied to the equations simultaneously, the results will be closer to reality and less simplification will be done in the equations.

since this paper examines a cold magnetized accretion-ejection structure, in addition to the need for the presence of a magnetic field, the magnetic field lines must have the necessary

curvature and can not be straight and an inclination of more than 30 degrees relative to the vertical axis is required for cold matter to escape [2].

Here, we examined two effects simultaneously. Since the vertical variation of angular velocity is ignored only if the magnetic field lines within the disk are almost straight and the magnetic field lines are not straight here, this vertical variation must be investigated. Then, the first effect is a deviation from the Keplerian rotation which enters the equations. Since we used the polytropic equation in the equations, the second effect is the study of gas with different polytropic indices. We considered gas in different states, monoatomic, diatomic, and isothermal, and studied the magnetized accretion-ejection structure in this state.

Our results show that in the presence of the polytropic equation and the deviation from Keplerian rotation, the process of mass reduction in the vertical direction for diatomic gas occurs faster than for other gases (Figure 5). For all gases, the variation in the toroidal magnetic field in the vertical direction (Figure 5) is similar. In [11], after initial widening, the flux tubes explicitly bend towards the jet axis, forcing the matter to flow along them but here this inclination is seen less. Furthermore, for a constant ejection rate, the monoatomic gas has a greater deviation from the Keplerian rotation (Figure 5), after that, the isothermal gas, and finally the diatomic gas. This deviation is reduced at the disk surface. Also, (Figure 5) for a smaller ejection rate (smaller $\zeta$), the deviation from the Keplerian rotation is greater. As we move up from the mid-plane, the mass flux moves to the top of the disk, which indicates that the mass exits in a vertical direction. The amount of mass flux output, in the vertical direction for different gamma values, does not show a significant difference.

We hope that this paper, which examines previous works from a different perspective, will help to explain some observational phenomena and provide benchmarks for numerical models.

# References

[1] Beckwith, K., Hawley, J. F., Krolik, J. H. 2008, ApJ., 678, 1180.

[2] Blandford, R. D., Payne, D. G. 1982, MNRAS., 199, 883.

[3] Casse, F. & Ferreira, J. 2000a, A&A., 353, 1115.

[4] Casse, F. & Ferreira, J. 2000b, A&A., 361, 1178.

[5] Casse, F. & Keppens, R. 2002, ApJ., 581, 988.

[6] Casse, F. & Keppens, R. 2004, ApJ., 601, 90.

[7] Fendt C. 2006, ApJ., 651, 272.

[8] Fendt, C. 2011, ApJ., 737, 43.

[9] Ferreira, J., Pelletier G. 1993, A&A., 276, 625.

[10] Ferreira, J., Pelletier G. 1993, A&A., 276, 637.

[11] Ferreira, J., Pelletier G. 1995, A&A., 295, 807.

[12] Ferreira, J. 1996, in W. Kundt (ed.), Jets from Stars and Galactic Nuclei, Springer-Verlag, Berlin.

[13] Ferreira, J. 1997, A&A., 319, 340.

[14] Jacquemin-Ide, J., Ferreira, J., Lesur, G. 2019, MNRAS.

[15] Kato, S. X., Kudoh, T. & Shibata, K. 2002, ApJ., 565, 1035.

[16] Li, Z. Y. 1995, ApJ., 444, 848.

[17] Li, Z. Y. 1996, ApJ., 465, 855.

[18] Liska, M. T. P., Tchekhovskoy, A., Quataert, E. 2018, arXiv eprints, p. arXiv:1809.04608.

[19] Pelletier, G., Pudritz, R. E. 1990, in C. Bertout, S. Collin-Souffrin, J.P. Lasota and J. Tran Thanh Van (eds.) Proc. I.A.P. coll., Structure and Emission Properties of Accretion Disks, Frontieres.

[20] Pelletier, G., Pudritz, R. E., Ferreira, J., Rosso, F. 1991, in J. Roland, H. Sol and G. Pelletier (eds.), Proc. I.A.P. coll., Extragalactic Radio Sources: From Beams to Jets, Cambridge Univ press.

[21] Pelletier, G., Pudritz, R. E. 1992, ApJ., 394, 117.

[22] Prasanna, A. R. 1982, Astr. Soc., 10, 205.

[23] Pringle, J. E. 1992, 3700 San Martin Drive, Baltimore, MD 21218, USA.

[24] Pudritz, R. E. 1985, ApJ., 293, 216.

[25] Uchida, Y. & Shibata, K. 1985, PASJ., 37, 515.

[26] Wardle, M., Konigl, A. 1993, ApJ., 410, 218.

[27] Zanni, C., Ferrari, A., Rosner, R., Bodo, G., Massaglia, S. 2007, A&A., 469, 811.

[28] Kudoh, T., Shibata, K., & Matsumoto, R. 1998, The central regions of the Galaxy and galaxies, Proceedings of the 184th symposium of the International Astronomical Union, held in Kyoto, Japan.

[29] Murphy, G. C., Ferreira, J., & Zanni, C. 2010, A&A., 12633.

[30] Sheikhnezami, S., Fendt, C., Porth, O., Vaidya, B., Ghanbari, J. 2012, arXiv:1207.6086v1.

[31] Stepanovs, D., Fendt, C. 2014, arXiv:1407.3136v1.

[32] Sheikhnezami, C., & Fendt, C. 2015, arXiv:1510.07645v1.

[33] Sheikhnezami, C., & Fendt, C. 2018, arXiv:1805.05962v1.

[34] Sheikhnezami, C., & Fendt, C. 2022, arXiv:2112.02111v1.

[35] Porth, O., Fendt, C. 2010, International Journal of Modern Physics, 19.

[36] Vaidya, B., Fendt, C., Beuther, H., & Porth, O. 2011, arXiv:1108.4924v1.

[37] Ouyed, R. 2003, Ap&SS., 287, 87.

[38] Romanova, M. M., Ustyugova, G. V., Koldoba, A. V., & Lovelace R. V. E. 2009, Mon. Not. R. Astron. Soc., 399, 1802.

[39] Mignone, A., Rossi, P., Bodo, G., Ferrari, A., & Massaglia, S. 2010, Monthly Notices of the Royal Astronomical Society, 402, 7.

[40] Gaibler, V., Khochfar, S., & Krause, M. 2011, Mon. Not. R. Astron. Soc., 411, 155.

[41] Porth, O. 2013, MNRAS., 429, 2482.

[42] Cielo, S., Antonuccio-Delogu, V., Maccio, A. V., Romeo, A. D., & Silk, J. 2014, MN-RAS., 439, 2903.

[43] Sheikhnezami, S., Abgharian-Afoushteh, M., ApJ., 883, 160.

[44] Lovelace, R. V. E., Wang, J. C. L., & Sulkanen, M. E. 1987, ApJ., 315, 504.

[45] Wang, J. C. L., Sulkanen, M. E., & Lovelace, R. V. E. 1990, ApJ., 355, 38.

[46] Wang, J. C. L., Sulkanen, M. E., & Lovelace, R. V. E. 1992, ApJ., 390, 46.

[47] Khanna, R., Camenzind, M. 1994, A&A., 263, 401.